Co-sputtered Pr 3+ -doped Ga-Ge-Sb-Se active waveguides for mid-infrared operation

Geoffrey Louvet, Simone Normani, Loïc Bodiou, Jan Gutwirth, Jonathan Lemaitre, Parastesh Pirasteh, Jean-Louis Doualan, Albane Benardais, Yannick Ledemi, Younes Messaddeq, et al.

Co-sputtered Pr^{3+}-doped Ga-Ge-Sb-Se active waveguides for mid-infrared operation

Geoffrey Louvet,[1,5] Simone Normani,[2] Loïc Bodiou,[3] Jan Gutwirth,[2] Jonathan Lemaitre,[3] Parastesh Pirasteh,[3] Jean-Louis Doualan,[4] Albane Benardais[1], Yannick Ledemi[5], Younes Messaddeq[5], Petr Němec,[2] Joël Charrier,[3] Virginie Nazabal[1,2*]

[1]*Univ Rennes, CNRS, ISCR (Institut des Sciences Chimiques de Rennes) – UMR 6226, F-35000 Rennes, France*
[2]*Department of Graphic Arts and Photophysics, Faculty of Chemical Technology, University of Pardubice, 53210 Pardubice, Czech Republic*
[3]*Univ Rennes, CNRS, Institut FOTON - UMR 6082, F-22305 Lannion, France*
[4]*CIMAP UMR-CNRS 6252, Université de Caen Normandie, 14050 Caen, France*
[5]*Centre d'Optique, Photonique et Laser (COPL), Université Laval, Québec, Canada*
**virginie.nazabal@univ-rennes1.fr*

Abstract: This work reports on the properties of luminescent waveguides based on quaternary Ga-Ge-Sb-Se amorphous thin films doped with praseodymium. The waveguides were fabricated *via* magnetron co-sputtering followed by inductively coupled plasma reactive ion etching. The initial thin films thickness and optical properties were assessed and the spectroscopic properties of the waveguides were measured. The measurements show promising results - it is possible to obtain mid-infrared fluorescence at 2.5 and 4.5 µm by injecting near infrared light at 1.5 µm as the pump beam. By comparing waveguides with various praseodymium concentrations, the optimal doping content for maximum fluorescence intensity was identified to be close to 4100 ppmw. Finally, correlation between the intensity of mid-infrared emission and the width/length of the waveguide is shown.

1. Introduction

Amorphous chalcogenides based on germanium (for example, Ge-Sb-Ch, Ga-Ge-Sb-Ch; Ch = S, Se, Te) are under deep investigation as host materials for infrared applications. The main reasons are their low phonon energies [1,2], high linear and nonlinear refractive indices [3,4] with relatively high transmittance extending well into the middle wavelength infrared (MWIR) spectral region [5], the possibility to deposit them as thin films with relative ease [6–9], and the solubility of rare earths within them [10,11]. The use of these optically active materials enables the manufacturing of performant waveguides and other photonic devices operating in the near to long wavelength infrared (NWIR-to-LWIR) range. A particular interest is given to the development of integrated continuum light sources that may rival and eventually replace the use of quantum cascade lasers and super-continuum lasers for integrated photonics [12,13]. High nonlinearities of amorphous chalcogenides make them very interesting for the development of broadband light sources for all-optical sensors as well as signal processing devices.

In addition to the nonlinear effects of chalcogenides to generate IR sources, rare earth-doped chalcogenides can also offer innovative solutions. Apart from erbium, rare earths such as dysprosium, praseodymium, terbium and samarium are considered as the most promising dopant ions for MWIR-to-LWIR emission and amplification, under NWIR excitation. Rare earth-doped chalcogenides fibers have already been successfully fabricated for remote monitoring applications [14]. Above all, these materials enable the detection of gases such as CO_2, CO, CH_4, $CHCl_3$ as well as obtaining emission around 7-8 µm when doped with dysprosium, terbium or samarium [15–17].

Besides, the manufacture of low optical loss rare earth-doped chalcogenide waveguides with efficient fluorescent emission and potentially light amplification has started to be reported in the last five years [18–20]. Among the manufacturing techniques, radio-frequency (RF) magnetron sputtering is a relatively easy process for the deposition of amorphous chalcogenide thin films [21]. Especially, the

properties of sputtered Ge-Sb-Se films have been thoroughly described in a previous work [8]. Here, Ge-based system was selected to avoid presence of toxic As while the addition of gallium is required to ensure a consistent and homogeneous rare earth ion incorporation in sputtered thin films. Thus for rare earth doping of sputtered thin films, the resulting host system selected is Ga-Ge-Sb-S(Se) [20,22]. Moreover, microdisk resonators based on erbium-doped chalcogenide thin films have been designed by Al Tal *et al.* [23], showing the potential for obtaining efficient MWIR coherent light generation at 4.5 µm. The simulations in the work of Palma *et al.* [24] provide encouraging results for the operation of praseodymium-doped chalcogenide microdisk resonators designed for emission at 4.7 µm, with the possibility of reaching higher slope efficiencies than with other rare earths, such as erbium. These studies paved the way for the development and fabrication of optical sensors and amplifiers with a large array of potential uses, from environmental monitoring to biomedical applications. However, while information on dysprosium- and praseodymium-doped chalcogenide fibers has been growing, there is still a lack of knowledge on the properties of rare earth-doped chalcogenide thin film-based structures for integrated applications.
Within the goal of obtaining optically active micro-structures, praseodymium doping is very appealing for mid-infrared applications [20,25,26] and it should be noted that despite weak branching ratio, laser operation at 5.2 and 7.2 µm has been reported in Pr^{3+}:$LaCl_3$ crystal [27]. Thanks to Pr^{3+} absorption bands, which allow efficient pumping in the near infrared at 1.55 µm with commercial laser sources or at about 2 µm, various radiative transitions lead to broad emissions centered on both 2.5 and 4.5 µm. However, despite the rather extensive information provided by the aforementioned literature, the data on the properties of chalcogenide-based waveguides are still rather scarce, particularly as it relates to their physical and chemical parameters such as doping concentration, waveguide length and width optima. Most of the available literature data deal with optically active chalcogenide waveguides exploiting erbium as the dopant ion [18,19,28]. Hence, it is necessary to provide a more complete description of such devices to maximize their performances.

The aim of this work is therefore to report a more complete description regarding performance of Ga-Ge-Sb-Se waveguides doped with Pr^{3+} ions fabricated by co-sputtering technique. Their optical and spectroscopic properties were compared as a function of their doping concentration and geometric parameters, with the final goal of providing a crucial step towards their optimization as efficient active optical integrated devices.

2. Methods

Two bulk glasses from Ga-Ge-Sb-Se quaternary system were fabricated by melt-quenching technique, heating the pure elements above the melting temperature in a furnace and then cooling the melt below the glass transition temperature, thus obtaining glass with a nominal composition of $Ga_5Ge_{20}Sb_{10}Se_{65}$. One of the bulks was doped with a praseodymium (10000 ppmw, parts per million by weight). Both glass cylinders were then cut into several slices each, obtaining the targets for sputtering (∅ = 50 mm), which were finally polished. Two undoped targets and one Pr^{3+}-doped target were mounted onto a three-cathode co-sputtering cluster in order to fabricate the thin films. Thin films were deposited at room temperature onto thermally oxidized (2 µm SiO_2 layer) single crystalline silicon substrates by magnetron co-sputtering using all three cathodes simultaneously. The Pr^{3+} doping concentration within each sample was tailored by adjusting the power applied to the different cathodes. The depositions took place under 10^{-2} mbar Ar pressure. The choice of deposition parameters was based on previous results with glass target of related compositions [8,29]. The deposition time was adapted to get films of ~1 µm thickness. The resulting thin films were estimated at Pr^{3+} concentrations of 1300, 2700, 4100, 6700, and 10000 ppmw, calculated by considering the sputtering rate of each individual cathode for each power selected for co-sputtering process of Pr^{3+}:GaGeSbSe thin films. Energy-dispersive X-ray spectroscopic (EDS) characterization was performed on the three targets (JSM 6400-OXFORD Link INCA collecting the spectra over a roughly 0.01 mm^2 area for each sample) and co-sputtered films using a scanning electron microscopy (SEM, TESCAN VEGA 3 EasyProbe) linked with an EDS analyzer. The standard uncertainty of

EDS measurements for thin film is ±1 at. %. Typically, the EDS estimates were averaged over measurements on three separate area per sample.

The thin films were analyzed by variable angle spectroscopic ellipsometry (VASE) from the UV to the LWIR range, in order to have an estimate of their thickness and refractive index. The UV-to-NWIR measurements were performed with a Woollam VASE vertical ellipsometer with a 20 nm step from 300 to 2300 nm, while the IR spectra were collected with a Woollam IR-VASE Mark II ellipsometer, ranging from 330 to 5900 cm^{-1} with an 8 cm^{-1} resolution. Refractive index, thickness and band-gap were determined from the ellipsometry data fitting using the Cody-Lorentz model and Sellmeier dispersion in UV-to-NIR and mid-infrared spectral ranges, respectively [30,31].

The optical field distribution of the propagating modes and the corresponding effective indices were simulated, at different wavelengths, for TE and TM polarizations, and for different ridge waveguide dimensions using a commercial mode solver (Fimmwave, Photon Design). These simulations were performed by considering ridge waveguides made of Pr^{3+}-doped $Ga_5Ge_{20}Sb_{10}Se_{65}$ guiding layer and SiO_2 confinement layers on Si substrate knowing their respective refractive index.

Several series of ridge waveguides with different widths were fabricated *via* inductively coupled plasma reactive ion etching (ICP-RIE) with the use of CHF_3 gas. The gas was injected into the chamber with a flow of 10 sccm, keeping the pressure set at $2.67 \cdot 10^{-3}$ mbar (2 mTorr) for the duration of the etching. The powers applied were 150 and 100 W for the plasma generation and the etching process, respectively. After the etching, the samples were cleaved to obtain the desired size for the optical measurements. These experiments resulted in a set of waveguides 6, 8, and 10 µm wide and 5, 6, and 10 mm long for each of the aforementioned Pr^{3+} concentrations.

Preliminary fluorescence measurements on the non-etched thin films were carried out by exciting the samples to the $^3F_4$ level focusing a 1.55 µm laser diode beam onto the surface, and collecting the normal emission intensity at 2.5 and 4.5 µm *via* a monochromator, exploiting a nitrogen-cooled InSb detector. Guided-light spectroscopic measurements were performed by injecting the waveguides with a 1.55 µm pump beam and collecting the emission spectra around 2.5 and 4.5 µm according to the known praseodymium energy level transitions. High pump power (up to 100 mW) was provided by a Highwave C band erbium-doped fiber-broadening source. A microlens at the output end of the fiber [32] allowed to inject directly into the waveguide. A fibered variable attenuator allows power dependent photoluminescence (PL) measurements. The emission was collected on the other side using a ZnSe microscope objective to focus the output light onto the entrance slit of a Horiba iHR320 monochromator, leading to a liquid nitrogen-cooled InSb detector (Teledyne Judson Technologies). To improve signal-to-noise ratio (SNR) of the MWIR PL, the detector output photocurrent was amplified by a low-noise transimpedance amplifier and recorded using a lock-in amplifier (Stanford Research Systems, SRS810). A removable mirror was also employed to assess the pump injection by deflecting the collected light onto an infrared camera and observing the guided mode. The spectra around 2.5 and 4.5 µm were collected using gratings blazed at 2 and 4 µm, with groove densities of 300 and 150 lines/mm respectively, and long-pass filters with cut-off wavelengths of 1900 nm and 3500 nm respectively to remove the pump residue and undesired luminescence. Measurements were performed at room temperature.

3. Results and discussion

3.1 Fabrication and characterization of Pr^{3+}:GaGeSbSe co-sputtered thin films

The chalcogenide thin films RF co-sputtering allowed the concentration of rare earth ions to be varied without having to modify the composition of the film, which remains very close, as can be seen in table 1, to the composition of the three targets: $Ga_{5.2}Ge_{19.9}Sb_{9.6}Se_{65.3}$ for the Pr^{3+}:GaGeSbSe glass target and $Ga_{5.0}Ge_{20.0}Sb_{9.6}Se_{65.4}$ (±0.5%) for the undoped targets. The power applied to the different cathodes, the deposition time for each sample, the thin film composition, the thin film thickness, and the band-gap energy values are summarized in table 1. The thickness of the deposited Pr^{3+}:GaGeSbSe thin films estimated through the ellipsometry measurements was found to be consistently between

920 and 990 nm (table 1). Their refractive index was determined as 2.59±0.02 at 1.55 µm (corresponding to the intended pump wavelength), 2.56±0.02 at 2.5 µm and 2.54±0.03 at 4.5 µm (the two wavelengths corresponding to the main MIR emissions of Pr^{3+}) when averaging refractive index values obtained for all five thin films. Relatively large error bars (±0.02 at 1.55 and 2.5 µm, ±0.03 at 4.5 µm) are mainly due to the film with highest Pr^{3+} content (10000 ppmw of Pr^{3+}) as this layer has larger refractive index than other films: 2.61, 2.58, and 2.57 at 1.55, 2.5, and 4.5 µm, respectively). One may see that the estimated band-gap energy seems to decrease slightly as the Pr^{3+} concentration increases. However, the behavior of refractive index and bang-gap energy can be correlated with both, Pr^{3+} concentration and gradual increase of Sb and Se percentage (and consequent slight reduction in Ga and Ge contents), observed in the samples composition.

Table 1. Summary of the RF co-sputtering deposition conditions and basic characteristics of Pr^{3+}:GaGeSbSe thin films using two undoped $Ga_5Ge_{20}Sb_{10}Se_{65}$ glass targets (cathode 2 and 3) and one $Ga_5Ge_{20}Sb_{10}Se_{65}$ doped with 10000 ppmw of Pr^{3+} (cathode 1).

	Cath. 1 10000 ppmw	Cath. 2 undoped	Cath. 3 undoped	Dep. time	Pr^{3+} estimated concentration	Thin films experimental composition	Thickness	Band-gap energy
Sample	*W*	*W*	*W*	*min*	*ppmw (±200 ppmw)*	*at. % (±1%)*	*nm (±10 nm)*	*eV (±0.01 eV)*
C-1	10	20	20	104	1300	$Ga_6Ge_{19}Sb_{10}Se_{65}$	950	1.82
C-2	20	20	20	82	2900	$Ga_5Ge_{19}Sb_{10}Se_{66}$	950	1.81
C-3	20	20	0	120	4100	$Ga_5Ge_{18}Sb_{11}Se_{66}$	990	1.79
C-4	20	10	0	194	6700	$Ga_5Ge_{18}Sb_{11}Se_{66}$	980	1.77
C-5	20	0	0	313	10000	$Ga_4Ge_{17}Sb_{12}Se_{67}$	920	1.76

3.2 Photoluminescence of Pr^{3+}:GaGeSbSe co-sputtered thin films

The spectroscopic properties of Pr^{3+} with respect to mid-infrared emissions in the 2-7 µm spectral region are relatively difficult to study given the multiple contribution from different transitions involving the thermalized levels ($^3F_4$, $^3F_3$) and ($^3F_2$, $^3H_6$), the $^3H_5$ level and the ground level $^3H_4$ [33]. In addition, the possible resonances between these levels conducive to energy transfers make it difficult to interpret the (de)population of the involved levels affecting their lifetime, the emission spectra shape and the intensity ratio between the emission lines [25,33–35]. The complete diagram of Pr^{3+} energy levels and possible transitions is represented in figure 1, highlighting the transition used for pumping and the ones that are expected to make up the emission spectra.

This task becomes thankless when the material is a thin film whose spectroscopic properties are even more difficult to characterize than those of bulk glass or optical fiber. Moreover, the size of the micro-system devices requires a consequently higher rare earth-doping level than what can be found in optical fibers of much greater length. As a result, non-radiative energy transfer processes between Pr^{3+} ions can become preponderant and profoundly affect the overall luminescence intensity and shape of these emission bands [25,33–35]. In addition to the MWIR radiative transitions (3300-1500 cm^{-1}) and energy transfers due to ion-ion interactions, Pr^{3+} ions may also exhibit interactions with host material vibrations, either intrinsic or extrinsic. It has been shown that the higher phonons energy accessible in the host matrix are generally the first involved in the multiphonon relaxation processes. Thus, impurities such as Se-H (2190 cm^{-1}) and Ge-H (2030 cm^{-1}) will play a major role, more important than the intrinsic phonons in the Ga-Ge-Sb-Se glass that extend between 175 and 300 cm^{-1} with a phonons density mainly centered between 200-225 cm^{-1} for active modes in Raman spectroscopy and 275-300 cm^{-1} for those in IR spectroscopy [15,36]. The extrinsic phonon vibrations of Se-H or Ge-H impurities resonant with the energy gaps of the MWIR transitions will forcibly induce an unfavorable migration and the concentration of these impurities should therefore be kept as low as possible in co-sputtered thin films and therefore the used glass targets [37].

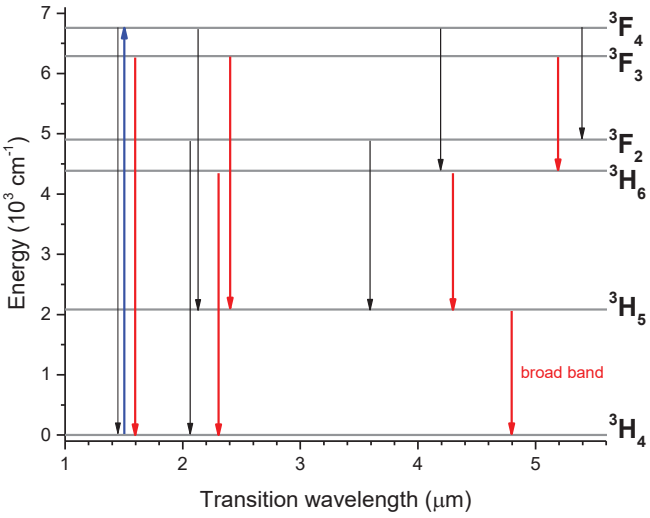

Fig. 1. Dieke diagram of the Pr^{3+} ion in Ga-Ge-Sb-Se glasses and possible radiative transitions between energy levels. The blue arrow highlights the transition used for pumping to the $^3F_4$ level and the black arrows represent the possible radiative transitions that arise from two thermalized levels with a low population rate.

The preliminary fluorescence spectra of the RF co-sputtered films with non-injected pump configuration were compared to that of a piece of 10000 ppmw Pr^{3+}-doped glass bulk as shown in figure 2 (the spectra are normalized to the respective peak intensity value of the 2.5 μm emission band). One can observe that both co-sputtered thin films and bulk glass doped with 10000 ppmw of Pr^{3+} share a similar spectral band shape at ~2.5 μm but there is a significant difference in the 3.5-5.5 μm emission, in particular in the long-wavelength part of the band.

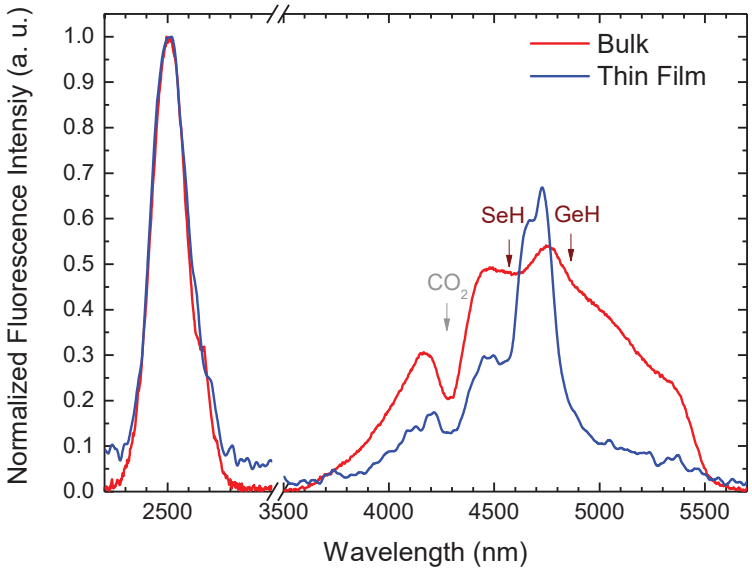

Fig. 2. IR fluorescence spectrum of Ga-Ge-Sb-Se thin film doped with 10000 ppmw of Pr^{3+} compared to that of corresponding bulk glass with excitation at 1.55 μm.

The first photoluminescence band of Pr^{3+} in the spectral range of 2-2.7 µm is usually related to different transitions, ($^3F_4$, $^3F_3$) → $^3H_5$ and ($^3F_2$, $^3H_6$) → $^3H_4$ (figure 1) [38]. However in this configuration with 10000 ppmw of Pr^{3+}, the shoulder expected at ~2.2 µm, that may be associated with the $^3F_4 \rightarrow {}^3H_5$ and $^3F_2 \rightarrow {}^3H_4$ transitions, is not clearly visible while the shoulder at 2.6 µm ($^3H_6 \rightarrow {}^3H_4$) in the right part of the main band centered at 2.5 µm ($^3F_3 \rightarrow {}^3H_5$) is better observed. It can be probably partially masked by noise and also related to the fact that the $^3H_6$ and $^3F_3$ manifolds are predominantly populated respecting Boltzmann's law - in particular, according to the Boltzmann distribution at room temperature, the $^3F_3$ level accounts for 88% of the total ($^3F_4$,$^3F_3$) manifold population, while the $^3H_6$ population is 97% of the combined ($^3F_2$,$^3H_6$) manifold for the $Ga_5Ge_{20}Sb_{10}Se_{65}$ matrix. In addition, the analysis for these two samples is more complex due to non-radiative relaxation involving such levels caused by Pr^{3+} concentration. Indeed, for such high concentration, energy transfers can be expected between two close Pr^{3+} ions depopulating the ($^3F_4$,$^3F_3$) or ($^3F_2$,$^3H_6$) thermalized levels. Three cross-relaxation processes have been proposed involving the following energy levels ($^3F_4$,$^3F_3$) : $^3H_5 \rightarrow$ ($^3F_2$,$^3H_6$) x2; ($^3F_4$,$^3F_3$) : $^3H_4 \rightarrow$ ($^3F_2$,$^3H_6$) : $^3H_5$, ($^3F_2$,$^3H_6$): $^3H_4 \rightarrow$ ($^3F_2$,$^3H_6$) : $^3H_5$ [34] and then one cross-relaxation ($^3F_2$,$^3H_6$) : $^3H_4 \rightarrow {}^3H_5$ x2 [25,35].
The photoluminescence between 3.5 and 5.5 µm is mainly composed of the transition ($^3F_2$, $^3H_6$) → $^3H_5$ (~3.5 and ~4.5 µm, respectively) and the transition $^3H_5 \rightarrow {}^3H_4$ (~4.7 µm) involving many Stark split manifolds at the origin of this extended bandwidth. The wide emission can also have contributions from transitions between ($^3F_4$, $^3F_3$) → ($^3F_2$, $^3H_6$) levels, especially at longer wavelengths [39,40]. Taking into account that at room temperature the population distribution of the thermally coupled ($^3F_4$, $^3F_3$) levels is 88%in the $^3F_3$ state [33] and due to its low branching ratio, the transition from $^3F_4$ to ($^3F_2$, $^3H_6$) emitting at ~5.4 µm is unlikely. The decreases in PL intensity around 4.3, 4.5 and 4.9 µm are, respectively, due to the absorption of CO_2 from the atmosphere and the absorption of Se-H and Ge-H impurities from the glass bulk and thin film, as previously mentioned. The difference observed may suggest that the bulk glass spectrum is more affected by strong $^3H_4 \rightarrow {}^3H_5$ reabsorption than the thin film, as can be classically seen by comparing PL in bulk glasses and fibers [41]. A variation in the structure surrounding the praseodymium ions in the co-sputtered thin films with respect to the bulk glass could also affect the ratio between the $^3H_6 \rightarrow {}^3H_5$ and $^3H_5 \rightarrow {}^3H_4$ main transitions. The changes may be possibly attributed to a combination of Stark splitting modification and cross-relaxation processes caused by a greater number of structural defects and Pr^{3+} clusters formation within the deposited layer as compared to the bulk [29]. In addition, the absorption of impurities that may be formed by the reactivity of the surface with the atmosphere like OH (2.9 µm), SeH (4.6 µm), GeH (4.9 µm), GeO (7.9µm) must play a more important role in the films than in bulk glasses, mainly due to the surface/volume ratio as shown in figure 2 with much more pronounced SeH and GeH absorption bands for the Pr^{3+} co-sputtered film. Another difference between bulk and film is the relative intensity of the two emission peaks: one can see that in the film sample, the 4.5 µm emission (integrated area of the emission band) is less intense with respect to the 2.5 µm fluorescence, as compared to the bulk. This indicates either a change in branching ratios or a very likely increase in energy migration to impurities.

3.3 Infrared emission of Pr^{3+}:GaGeSbSe rib waveguide

A set of the ridge waveguides obtained from the co-sputtered films by means of the ICP-RIE process is exemplified in figure 3. The major difficulty lies in the presence of gallium in the co-sputtered thin films, which is less suitable for etching with fluorinated gases than the other elements (Ge, Sb, Se), whose etching process was studied with the identification of etching products and plasma/glass interaction (Ge-Sb-Se) thin films in SF_6 and SF_6/Ar plasmas [42]. The resulting waveguides were designed to be multimode with respect to all wavelengths of interest, up to 5 microns at least, in order to increase the coupling efficiency and transmission (see figure 4). The pumping is distributed over the entire cross-section of the waveguide given the number of modes propagating at 1.55 µm, an approximation also used by A.L. Pelé *et al.* [43] and for an emission at 4.5 µm in the same way, many modes may be involved and therefore the measurement of optical losses would be made

extremely complex and uncertain by the lack of knowledge of the mode(s) detected. In the case of sulphide-based waveguides, doping with Er^{3+} ions and the incorporation of 5 at.% Ga in a Ge-Sb-S sputtered thin film has been shown to have little effect on the optical propagation losses [18]. The losses were found in both case to be slightly less than 1dB/cm at 1.55µm [44]. In addition, propagation losses values of the same order of magnitude (2.5 dB/cm) were demonstrated in the mid-IR (λ=7.7µm) for Ge-Sb-Se sputtered thin film [45]. If this statement could be extended to selenide-based waveguides, the actual losses of the waveguides mentioned in the manuscript should also be of the order of a few dB/cm.

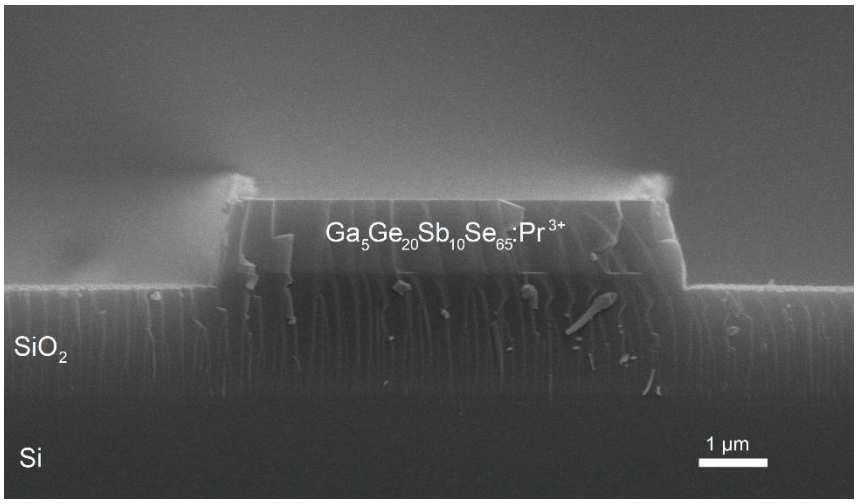

Fig. 3. An example of SEM image of a cross-section of $Ga_5Ge_{20}Sb_{10}Se_{65}:Pr^{3+}$ ridge waveguide co-sputtered on SiO_2/Si substrate.

The infrared emissions at both 2.5 and 4.5 µm were observed with light injection and the dependency of the output fluorescence intensity as a function of the different variables was studied. First, one should identify the most favorable conditions for efficient fluorescence depending on rare earth doping concentration: in particular, the Pr^{3+} content should be such that absorption and subsequent fluorescent emission are maximal, while minimizing the effects of optical quenching and reabsorption. We could notice that the shape of the 2-2.7 µm emission spectrum changes very little with concentration except that the shoulder at 2.2 µm is slightly less discernible in contrast to that at 2.6 µm on thin films with a Pr^{3+} concentration higher than 4100 ppmw.

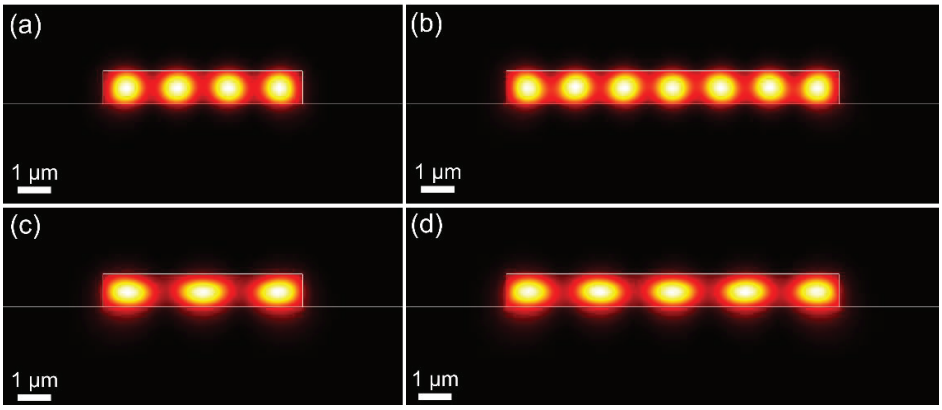

Fig. 4. Intensity mode profiles simulated at a wavelength of 4.5 µm in 6 µm and 10 µm wide waveguides for: (a) TE4, (b) TE7, (c) TM3, and (d) TM5 modes.

One can see from figure 5 that the optimal waveguide doping content allowing the most intense emission is 4100 ppmw of Pr^{3+}. The intensity behavior is similar at both 2.5 and 4.5 µm, but one can see that the intensity ratios among the samples are different for the two transitions. This might suggest a difference in the propagation efficiency for the two emissions in different samples related to absorption of the ground state depending on the Pr^{3+} concentration of the waveguide, although it is hard to give a definite conclusion due to the generally low signal-to-noise ratio of this emission band. Given these results, the following measurements for the assessment of fluorescence dependency on the other parameters were performed within 4100 ppmw Pr^{3+}-doped waveguides.

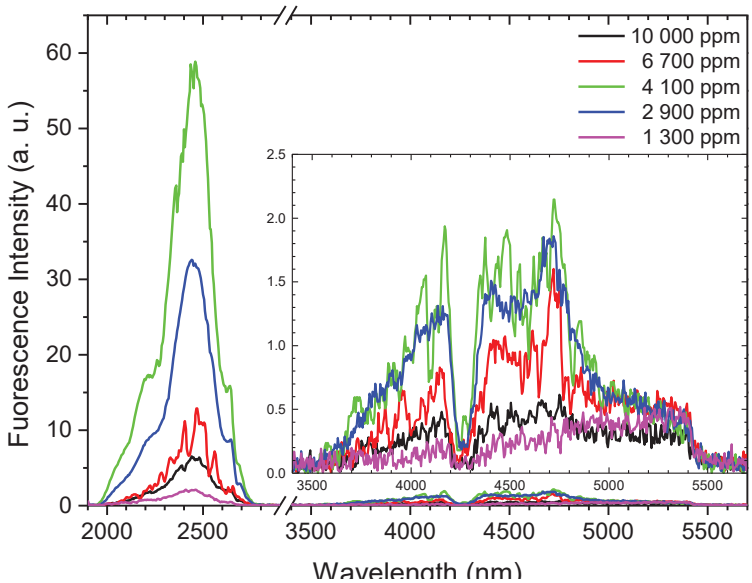

Fig. 5. MIR emission spectra collected at the output of the 8 µm (width) waveguides with length of 5 mm showing the fluorescence bands of Pr^{3+} at 2.5 and 4.5 µm with excitation at 1.55 µm.

One can see from figure 5 that the optimal waveguide doping content allowing the most intense emission is 4100 ppmw of Pr^{3+}. The intensity behavior is similar at both 2.5 and 4.5 µm, but one can see that the intensity ratios among the samples are different for the two transitions. This might suggest a difference in the propagation efficiency for the two emissions in different samples related to absorption of the ground state depending on the Pr^{3+} concentration of the waveguide, although it is hard to give a definite conclusion due to the generally low signal-to-noise ratio of this emission band. Given these results, the following measurements for the assessment of fluorescence dependency on the other parameters were performed within 4100 ppmw Pr^{3+}-doped waveguides.

The signal-to-noise ratio of the 4.5 µm emission is too low to investigate in close detail the band shape behavior *versus* the waveguide geometrical parameters, but some conclusions can be obtained from that of the 2.5 µm emission band. The study of emission intensity and band shape as a function of waveguide width is shown in figure 6.

Under the same excitation conditions and injecting the pump into the shortest waveguides in each set, the most intense fluorescence at 2.5 µm was observed for the 8 µm wide samples, which is thought to be mainly due to the higher pump beam coupling efficiency. Differences however become increasingly evident when changing the investigated waveguide length. In particular, under equal pump power, one may observe that in the case of the 6 µm width, the maximum emission intensity is obtained from the shortest waveguide (5 mm), while in the 8 µm wide case, the highest emission intensity was recorded when injecting into longer waveguides, particularly the one of 10 mm length (figure 7).

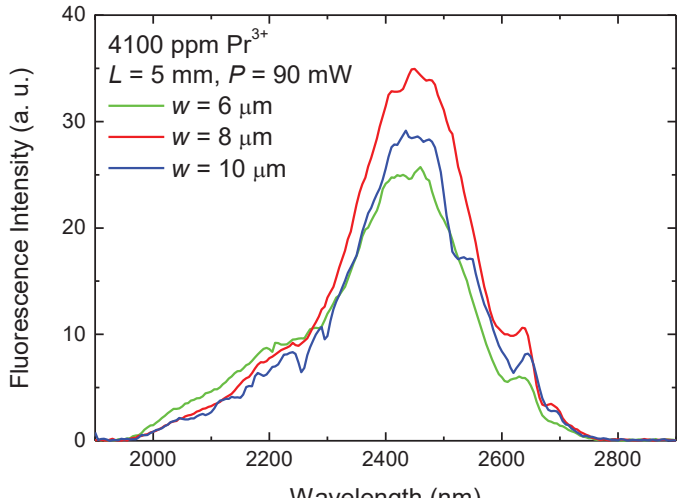

Fig. 6. Plot of the emission spectra of the 5 mm long waveguide showing the variation in intensity and band shape as a function of waveguide width.

The emission intensity increase with waveguide length observed in the 8 μm wide waveguide means that, within the values considered, the gain exceeds optical losses coming from both leaks and reabsorption processes. This behavior may suggest that the confinement of the fluorescence light is more efficient in the wider waveguides, as higher propagation losses could explain the drop in intensity with increasing length for the narrower samples. No noticeable red-shift in the emission spectra with respect to the shape of the thin film emission band for comparable Pr^{3+} concentration suggest no major contribution from radiation trapping, unlike Er^{3+}-doped chalcogenide glasses [46].

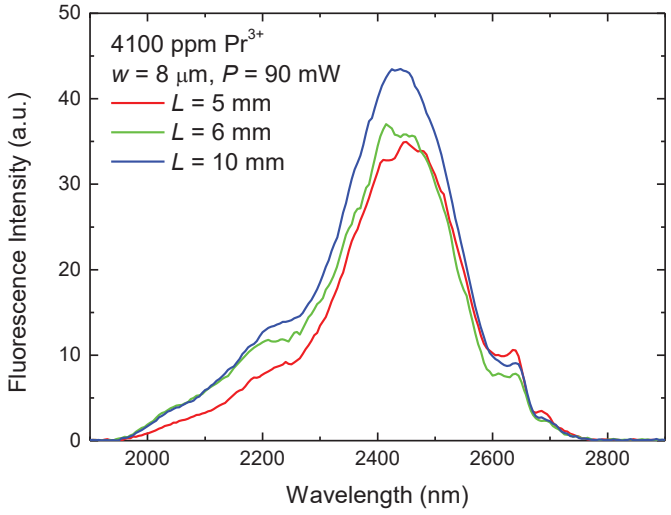

Fig. 7. Plot of the emission spectra of the 8 μm wide waveguide showing the variation in intensity and band shape as a function of waveguide length.

The fluorescence emission spectra at ~2.5 μm under different excitation powers were collected (figure 8a) for the 4100 ppmw Pr^{3+}-doped, 8 μm wide waveguide of 5 mm length. Figure 8c shows the comparison between the normalized 2.5 μm fluorescence spectra: as the band shape does not show any significant variation, no discernible effect of the pump power on the spectroscopy other than the increase in emission intensity can be observed. This means that the intensity ratio between the different IR emission transitions is apparently unaffected by the pump light intensity in the case

of Pr^{3+} co-sputtered samples. The peak intensity was then plotted as a function of incident pump power, as shown in figure 8b. As can be expected, the graph shows a monotone increase of fluorescence intensity, with a gradually decreasing slope indicative of the absorption saturation.

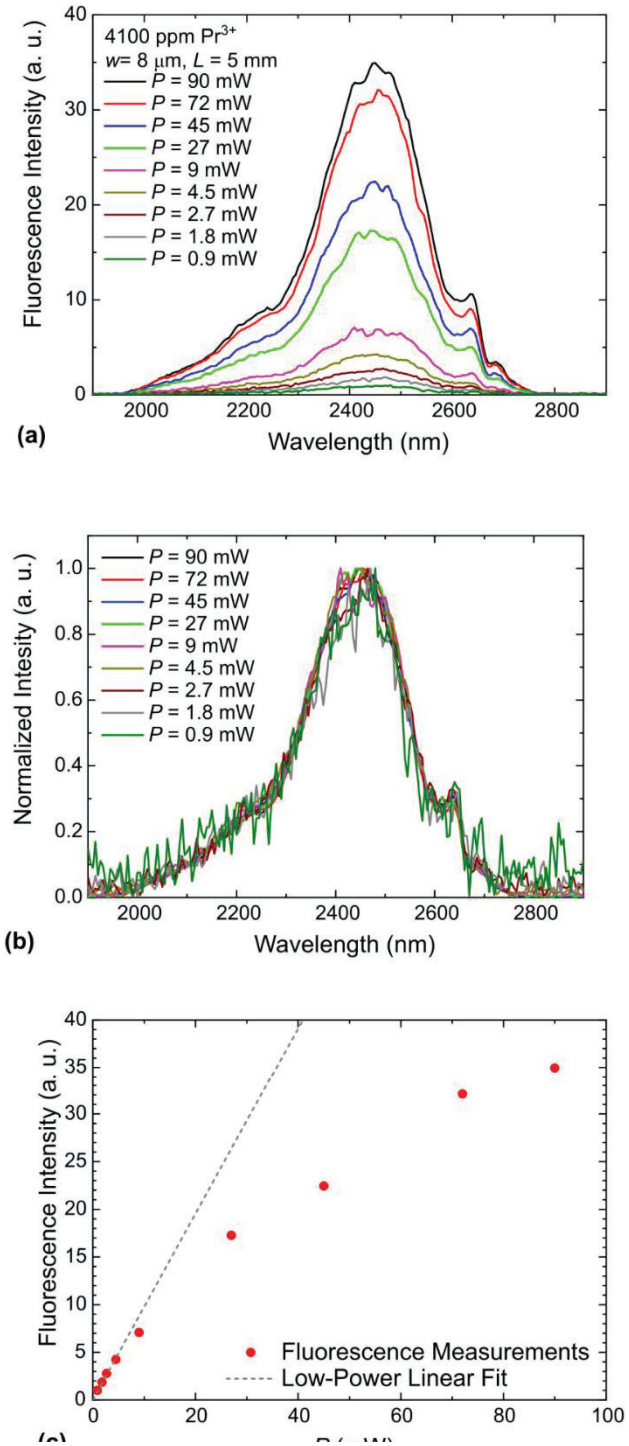

Fig. 8. Plot of the fluorescence spectra at ~2.5 µm showing the comparison of (a) intensity and (b) band shape as varying pump power, and (c) plot of the peak intensity as a function of pump power.

4. Conclusions

Praseodymium-doped Ga-Ge-Sb-Se co-sputtered waveguides have been proved a valid medium for the generation and propagation of infrared signal, and are therefore promising devices for NWIR and MWIR sensing and light amplification [47]. In particular, relatively wide ones are the most performant, as demonstrated by 8 µm-width waveguides having the highest output signal intensity, allowing for efficient infrared light emission and propagation even along 1 centimeter-long paths, and without deformation of the 2.5 µm emission band shape. By comparing waveguides with various praseodymium concentrations, the optimal doping for maximum fluorescence intensity was identified to be close to 4100 ppmw, where the most intense emission was recorded at both 2.5 and 4.5 µm wavelengths. These results provide a good overview of the main optical properties of fabricated structures as a function of the manufacturing parameters, which in turn opens the way for further investigation in order to fine-tune the operating features of such rare earth-doped quaternary chalcogenide waveguides, with the purpose of developing novel infrared active devices for potential environmental, biomedical and telecommunication applications.

Funding, acknowledgments, and disclosures

Funding

The authors would like to thank to the CNRS, the Brittany Region and Canadian Excellence Research Chair program (CERC) in Photonics Innovations for PhD funds, the project of International Mobility of Researchers at the University of Pardubice (OP RDE project CZ.02.2.69/0.0/0.0/16_027/0008008), to Czech Science Foundation (project No. 19-24516S) as well as to COST MP1401-STSM.

Acknowledgements

Technological processing of ridge waveguides was performed in the CCLO-Renatech clean room facilities of Institut Foton. Equipment funding of Institut Foton and CCLO was partly provided by the CPER Sophie. Incitative project

Disclosures

The authors declare no competing interests.

References

1. L. B. Shaw, B. Cole, P. A. Thielen, J. S. Sanghera, and I. D. Aggarwal, "Mid-wave IR and long-wave IR laser potential of rare-earth doped chalcogenide glass fiber," IEEE J. Quantum Electron. **37**(9), 1127–1137 (2001).
2. B. J. Park, H. S. Seo, J. T. Ahn, Y. G. Choi, J. Heo, and W. J. Chung, "Dy^{3+} doped Ge-Ga-Sb-Se glasses and optical fibers for the mid-IR gain media," Journal of the Ceramic Society of Japan **116**(1358), 1087–1091 (2008).
3. T. Kuriakose, E. Baudet, T. Halenkovič, M. M. R. Elsawy, P. Němec, V. Nazabal, G. Renversez, and M. Chauvet, "Measurement of ultrafast optical Kerr effect of Ge–Sb–Se chalcogenide slab waveguides by the beam self-trapping technique," Optics Communications **403**, 352–357 (2017).
4. T. Halenkovič, J. Gutwirth, T. Kuriakose, M. Bouška, M. Chauvet, G. Renversez, P. Němec, and V. Nazabal, "Linear and nonlinear optical properties of co-sputtered Ge-Sb-Se amorphous thin films," Optics Letters **45**(6), 1523–1526 (2020).
5. J.-L. Adam and X. H. Zhang, *Chalcogenide Glasses: Preparation, Properties and Application.*, No. 44 (Woodhead Publishing Series in Electronic and Optical Materials, 2014).
6. S. Ramachandran and S. G. Bishop, "Excitation of Er^{3+} emission by host glass absorption in sputtered films of Er-doped $Ge_{10}As_{40}Se_{25}S_{25}$ glass," Appl. Phys. Lett. **73**(22), 3196–3198 (1998).
7. C. Vigreux, R. Escalier, A. Pradel, L. Bastard, J.-E. Broquin, X. Zhang, T. Billeton, G. Parent, M. Barillot, and V. Kirschner, "Telluride buried channel waveguides operating from 6 to 20 µm for photonic applications," Optical Materials **49**, 218–223 (2015).
8. E. Baudet, M. Sergent, P. Němec, C. Cardinaud, E. Rinnert, K. Michel, L. Jouany, B. Bureau, and V. Nazabal, "Experimental design approach for deposition optimization of RF sputtered chalcogenide thin films devoted to environmental optical sensors," Sci Rep **7**(3500), 1–14 (2017).

9. B. Shen, H. Lin, S. Sharif Azadeh, J. Nojic, M. Kang, F. Merget, K. A. Richardson, J. Hu, and J. Witzens, "Reconfigurable Frequency-Selective Resonance Splitting in Chalcogenide Microring Resonators," ACS Photonics **7**(2), 499–511 (2020).
10. B. G. Aitken, C. W. Ponader, and R. S. Quimby, "Clustering of rare earths in GeAs sulfide glass," C. R. Chim. **5**(12), 865–872 (2002).
11. R. Chahal, F. Starecki, J.-L. Doualan, P. Němec, A. Trapananti, C. Prestipino, G. Tricot, C. Boussard-Pledel, K. Michel, A. Braud, P. Camy, J.-L. Adam, B. Bureau, and V. Nazabal, "Nd $^{3+}$:Ga-Ge-Sb-S glasses and fibers for luminescence in mid-IR: synthesis, structural characterization and rare earth spectroscopy," Opt. Mater. Express **8**(6), 1650–1671 (2018).
12. Y. Yu, X. Gai, P. Ma, K. Vu, Z. Yang, R. Wang, D.-Y. Choi, S. Madden, and B. Luther-Davies, "Experimental demonstration of linearly polarized 2–10 μm supercontinuum generation in a chalcogenide rib waveguide," Opt. Lett. **41**(5), 958–961 (2016).
13. M. Sinobad, C. Monat, B. Luther-Davies, P. Ma, S. Madden, D. J. Moss, A. Mitchell, D. Allioux, R. Orobtchouk, S. Boutami, J.-M. Hartmann, J.-M. Fedeli, and C. Grillet, "Mid-infrared octave spanning supercontinuum generation to 85 μm in silicon-germanium waveguides," Optica **5**(4), 360–366 (2018).
14. F. Starecki, A. Braud, J.-L. Doualan, J. Ari, C. Boussard-Plédel, K. Michel, V. Nazabal, and P. Camy, "All-optical carbon dioxide remote sensing using rare earth doped chalcogenide fibers," Optics and Lasers in Engineering **122**, 328–334 (2019).
15. N. Abdellaoui, F. Starecki, C. Boussard-Pledel, Y. Shpotyuk, J.-L. Doualan, A. Braud, E. Baudet, P. Nemec, F. Cheviré, M. Dussauze, B. Bureau, P. Camy, and V. Nazabal, "Tb^{3+} doped $Ga_5Ge_{20}Sb_{10}Se_{65-x}Te_x$ (x = 0-37.5) chalcogenide glasses and fibers for MWIR and LWIR emissions," Opt. Mater. Express **8**(9), 2887–2900 (2018).
16. F. Starecki, A. Braud, N. Abdellaoui, J.-L. Doualan, C. Boussard-Plédel, B. Bureau, P. Camy, and V. Nazabal, "7 to 8 μm emission from Sm^{3+} doped selenide fibers," Opt. Express **26**(20), 26462–26469 (2018).
17. F. Starecki, G. Louvet, J. Ari, A. Braud, J.-L. Doualan, R. Chahal, I. Hafienne, C. Boussard-Plédel, V. Nazabal, and P. Camy, "Dy^{3+} doped GaGeSbSe fiber long-wave infrared emission," Journal of Luminescence **218**(116853), (2020).
18. V. Nazabal, F. Starecki, J.-L. Doualan, P. Němec, P. Camy, H. Lhermite, L. Bodiou, M. L. Anne, J. Charrier, and J. L. Adam, "Luminescence at 2.8 μm: Er^{3+}-doped chalcogenide micro-waveguide," Optical Materials **58**, 390–397 (2016).
19. K. Yan, K. Vu, R. Wang, and S. Madden, "Greater than 50% inversion in Erbium doped Chalcogenide waveguides," Opt. Express **24**(20), 23304–23313 (2016).
20. L. Bodiou, F. Starecki, J. Lemaitre, V. Nazabal, J.-L. Doualan, E. Baudet, R. Chahal, A. Gutierrez-Arroyo, Y. Dumeige, I. Hardy, A. Braud, R. Soulard, P. Camy, P. Němec, G. Palma, F. Prudenzano, and J. Charrier, "Mid-infrared guided photoluminescence from integrated Pr^{3+}-doped selenide ridge waveguides," Optical Materials **75**, 109–115 (2018).
21. V. Nazabal and P. Němec, "Chapter 37 - Amorphous Thin Film Deposition," in *Springer Handbook of Glass, J. D. Musgraves, J. J. Hu, and L. Calvez* (Springer, Cham, 2019), pp. 1291–1330.
22. V. Nazabal, A.-M. Jurdyc, P. Němec, M.-L. Brandily-Anne, L. Petit, K. Richardson, P. Vinatier, C. Bousquet, T. Cardinal, S. Pechev, and J.-L. Adam, "Amorphous Tm^{3+} doped sulfide thin films fabricated by sputtering," Optical Materials **33**(2), 220–226 (2010).
23. F. Al Tal, C. Dimas, J. Hu, A. Agarwal, and L. C. Kimerling, "Simulation of an erbium-doped chalcogenide micro-disk mid-infrared laser source," Opt. Express **19**(13), 11951–11962 (2011).
24. G. Palma, M. C. Falconi, F. Starecki, V. Nazabal, J. Ari, L. Bodiou, J. Charrier, Y. Dumeige, E. Baudet, and F. Prudenzano, "Design of praseodymium-doped chalcogenide micro-disk emitting at 4.7 μm," Opt. Express **25**(6), 7014–7030 (2017).
25. M. F. Churbanov, B. I. Denker, B. I. Galagan, V. V. Koltashev, V. G. Plotnichenko, S. E. Sverchkov, M. V. Sukhanov, and A. P. Velmuzhov, "Peculiarities of 16-75 μm Pr^{3+} luminescence in $Ge_{36}Ga_5Se_{59}$ glass," Opt. Mater. Express **9**(11), 4154–4164 (2019).
26. L. Sojka, Z. Tang, D. Jayasuriya, M. Shen, J. Nunes, D. Furniss, M. Farries, T. M. Benson, A. B. Seddon, and S. Sujecki, "Milliwatt-Level Spontaneous Emission Across the 3.5–8 μm Spectral Region from Pr^{3+} Doped Selenide Chalcogenide Fiber Pumped with a Laser Diode," Applied Sciences **10**(2), 539–549 (2020).
27. S. R. Bowman, L. B. Shaw, B. J. Feldman, and J. Ganem, "A seven micron solid-state laser," in *Optical Society of America*, OSA Proceedings Series (B. Chai and S. Payne, 1995), **24**.
28. J. A. Frantz, J. S. Sanghera, L. B. Shaw, G. Villalobos, I. D. Aggarwal, and D. W. Hewak, "Sputtered films of Er^{3+}-doped gallium lanthanum sulfide glass," Materials Letters **60**(11), 1350–1353 (2006).
29. S. Normani, G. Louvet, E. Baudet, M. Bouška, J. Gutwirth, F. Starecki, J.-L. Doualan, Y. Ledemi, Y. Messaddeq, J.-L. Adam, P. Němec, and V. Nazabal, "Comparative study of Er^{3+}-doped Ga-Ge-Sb-S thin films fabricated by sputtering and pulsed laser deposition," Scientific Reports **10**(7997), (2020).
30. A. S. Ferlauto, G. M. Ferreira, J. M. Pearce, C. R. Wronski, R. W. Collins, X. Deng, and G. Ganguly, "Analytical model for the optical functions of amorphous semiconductors from the near-infrared to ultraviolet: Applications in thin film photovoltaics," Journal of Applied Physics **92**(5), 2424–2436 (2002).
31. P. Němec, M. Olivier, E. Baudet, A. Kalendová, P. Benda, and V. Nazabal, "Optical properties of $(GeSe_2)_{100-x}(Sb_2Se_3)_x$ glasses in near- and middle-infrared spectral regions," Materials Research Bulletin **51**, 176–179 (2014).

32. S. D. Le, E. Delcourt, P. Girault, A. Gutierrez-Arroyo, P. Azuelos, N. Lorrain, L. Bodiou, L. Poffo, J.-M. Goujon, Y. Dumeige, I. Hardy, P. Rochard, J. Lemaitre, P. Pirasteh, M. Guendouz, T. Chartier, L. Quétel, S. Claudot, J. Charrier, and M. Thual, "Study of Optimized Coupling Based on Micro-lensed Fibers for Fibers and Photonic Integrated Circuits in the Framework of Telecommunications and Sensing Applications," Comm. Phys. **26**(4), 325–334 (2017).
33. L. Shaw, B. Harbison, B. Cole, J. Sanghera, and I. Aggarwal, "Spectroscopy of the IR transitions in Pr^{3+} doped heavy metal selenide glasses," Opt. Express **1**(4), 87–96 (1997).
34. Y. G. Choi, B. J. Park, K. H. Kim, and J. Heo, "Crossrelaxations between and multiphonon relaxation of near-infrared excited states of Pr^{3+} ions in selenide glasses," Chemical Physics Letters **368**(5–6), 625–629 (2003).
35. B. J. Park, H. S. Seo, J. T. Ahn, Y. G. Choi, D. Y. Jeon, and W. J. Chung, "Mid-infrared (3.5–5.5μm) spectroscopic properties of Pr^{3+}-doped Ge–Ga–Sb–Se glasses and optical fibers," Journal of Luminescence **128**(10), 1617–1622 (2008).
36. V. Nazabal, P. Němec, A. M. Jurdyc, S. Zhang, F. Charpentier, H. Lhermite, J. Charrier, J. P. Guin, A. Moreac, M. Frumar, and J.-L. Adam, "Optical waveguide based on amorphous Er^{3+}-doped Ga–Ge–Sb–S(Se) pulsed laser deposited thin films," Thin Solid Films **518**(17), 4941–4947 (2010).
37. V. Moizan, V. Nazabal, J. Troles, P. Houizot, J.-L. Adam, J.-L. Doualan, R. Moncorgé, F. Smektala, G. Gadret, S. Pitois, and G. Canat, "Er^{3+}-doped GeGaSbS glasses for mid-IR fibre laser application: Synthesis and rare earth spectroscopy," Optical Materials **31**(1), 39–46 (2008).
38. P. Sourková, B. Frumarova, M. Frumar, P. Nemec, M. Kincl, V. Nazabal, V. Moizan, J.-L. Doualan, and R. Moncorgé, "Spectroscopy of infrared transitions of Pr^{3+} ions in Ga–Ge–Sb–Se glasses," Journal of Luminescence **129**(10), 1148–1153 (2009).
39. A. Ferrier, M. Velázquez, J.-L. Doualan, and R. Moncorgé, "Pr^{3+}-doped Tl_3PbBr_5: a non-hygroscopic, non-linear and low-energy phonon single crystal for the mid-infrared laser application," Appl. Phys. B **95**(2), 287–291 (2009).
40. H. Sakr, D. Furniss, Z. Tang, L. Sojka, N. A. Moneim, E. Barney, S. Sujecki, T. M. Benson, and A. B. Seddon, "Superior photoluminescence (PL) of Pr^{3+}-In, compared to Pr^{3+}-Ga, selenide-chalcogenide bulk glasses and PL of optically-clad fiber," Opt. Express **22**(18), 21236–21252 (2014).
41. R. Chahal, F. Starecki, C. Boussard-Plédel, J.-L. Doualan, K. Michel, L. Brilland, A. Braud, P. Camy, B. Bureau, and V. Nazabal, "Fiber evanescent wave spectroscopy based on IR fluorescent chalcogenide fibers," Sensors and Actuators B: Chemical **229**, 209–216 (2016).
42. T. Meyer, A. Girard, G. Le Dain, A. Rhallabi, E. Baudet, V. Nazabal, P. Němec, and C. Cardinaud, "Surface composition and micromasking effect during the etching of amorphous Ge-Sb-Se thin films in SF_6 and SF_6/Ar plasmas," Applied Surface Science (submitted), (2020).
43. A. L. Pelé, A. Braud, J. L. Doualan, F. Starecki, V. Nazabal, R. Chahal, C. Boussard-Plédel, B. Bureau, R. Moncorgé, and P. Camy, "Dy^{3+} doped GeGaSbS fluorescent fiber at 4.4 μm for optical gas sensing: Comparison of simulation and experiment," Optical Materials **61**, 37–44 (2016).
44. J. Charrier, M. L. Anne, H. Lhermite, V. Nazabal, J. P. Guin, F. Charpentier, T. Jouan, F. Henrio, D. Bosc, and J. L. Adam, "Sulphide $Ga_xGe_{25-x}Sb_{10}S_{65}$(x=0,5) sputtered films: Fabrication and optical characterizations of planar and rib optical waveguides," J. Appl. Phys. **104**, 073110 (2008).
45. A. Gutierrez-Arroyo, E. Baudet, L. Bodiou, V. Nazabal, E. Rinnert, K. Michel, B. Bureau, F. Colas, and J. Charrier, "Theoretical study of an evanescent optical integrated sensor for multipurpose detection of gases and liquids in the Mid-Infrared," Sensors and Actuators B: Chemical **242**, 842–848 (2017).
46. C. Koughia, C. Craig, D. W. Hewak, and S. Kasap, "Radiation trapping in selected Er^{3+} doped chalcogenide glasses and the extraction of the nonradiative lifetime," Opt. Mater. Express **9**(5), 2368 (2019).
47. L. Bodiou, Y. Dumeige, S. Normani, G. Louvet, P. Němec, V. Nazabal, and J. Charrier, " Design of a multimode interferometer-based mid-infrared multispecies gas sensor ", IEEE Sensors, 2020, 10.1109/JSEN.2020.3005346